Supporting Information

Unlocking the Potential of NiV-LDH@Mn_2O_3 Heterostructure via Band gap Modulation for Enhanced Water Splitting

Ragunath Madhu,[a,b] and Subrata Kundu[a,b,*]

[a]*Academy of Scientific and Innovative Research (AcSIR), Ghaziabad-201002, India.*

[b]*Electrochemical Process Engineering (EPE) Division, CSIR-Central Electrochemical Research Institute (CECRI), Karaikudi-630003, Tamil Nadu, India.*

*To whom correspondence should be addressed, *E-mail:* skundu@cecri.res.in; kundu.subrata@gmail.com. Phone/Fax: (+ 91) 4565-241487.

This file contains 27 pages in which the information on reagents and instruments used in the study, electrochemical measurements, surface charge determination, XRD, XPS, and other electrochemical calculations like redox behaviour, ECSA, C_{dl} values, comparison table, references etc., are given respectively.

Number of Figures: 14 (S1-S15)

Number of Tables: 3 (S1-S3)

Experimental Section

Reagents used

Manganese nitrate tetrahydrate ($Mn(NO_3)_2.4H_2O$), nickel chloride ($NiCl_2$), vanadium chloride (VCl_3), urea (NH_2CONH_2), ammonium fluoride (NH_4F) were purchased from the Sigma-Aldrich and used as received. Deionized water (DI) is used throughout this work.

Synthesis of flower-like Mn_2O_3

Mn_2O_3 were synthesized by hydrothermal process. For a typical synthesis, 5 mmol of $Mn(NO_3)_2.4H_2O$ was dissolved in a 30 mL of DI water. Further, 10 mmol of NH_4F and 25 mmol of urea (NH_2CONH_2) were added to the same solution and transferred to Teflon-lined autoclave. To this dissolved precursor, surface cleaned 2 × 2 nickel foam (NF) was kept inside and sealed properly. The autoclave kept for 6 h at a temperature of 120 °C in a hot air oven. After the completion of reaction the in-situ grown $Mn(OH)_2$ was cleaned several times with DI water and dried at 60 °C. Then the $Mn(OH)_2$@NF was subjected for annealing at 350 °C for 4 h in an air atmosphere to yield an Mn_2O_3. The obtained Mn_2O_3@NF was used for formation of heterostructure with the NiV-LDH.

Synthesis of heterostructured NiV-LDH@Mn_2O_3

The heterostructured NiV-LDH@Mn_2O_3 was synthesized through a hydrothermal treatment for 12 h. In a typical synthetic procedure, 175 mg of of $NiCl_2$, 0.039 mg VCl_3, 350 mg of urea and a pinch of NH_4F was dispersed in 30 mL of DI water. To this disperse solution in-situ grown Mn_2O_3@NF was immersed in a Teflon-lined stainless-steel autoclave and kept at 120 °C for 12 h. The obtained NiV-LDH@Mn_2O_3 was washed several times with water-ethanol mixture and dried in hot air oven at 60 °C for 12 h. Finally, all the obtained product was used as electrocatalyst for OER, HER and overall water splitting reaction.

Synthesis of NiV-LDH

For comparison, NiV-LDH@NF was synthesized by using the above similar procedure without the inclusion of in-situ grown Mn_2O_3@NF in a Teflon-lined stainless-steel autoclave.

Characterization techniques

The as-prepared samples are initially subjected to XRD analysis with a scanning rate of 5° min^{-1} in the 2θ range 10-80° using a Bruker X-ray powder diffractometer (XRD) with Cu Kα radiation (λ = 0.154 nm). The morphology of the catalysts was characterized with FE-SEM instrument (SUPRA 55VP Carl Zeiss) with a separate EDS detector connected to that instrument. Energy Dispersive X-ray Spectroscopy (EDS) analysis was done with the assistance of FE-SEM instrument. X-ray photoelectron spectroscopic (XPS) analysis was performed using a Theta Probe AR-XPS system (Thermo Fisher Scientific, UK). HR-TEM, (TecnaiTM G2 TF20) working at an accelerating voltage of 200 kV and by Talos F-200-S with HAADF elemental mapping.

Electrochemical measurements

The electrochemical properties were measured using a Metrohm AUTOLAB-M240 instrument with techniques like CV, LSV, and chronoamperometry. All the electrochemical experiments were carried out by employing a conventional three-electrode set-up. The in-situ modified NiV-LDH@Mn_2O_3, Mn_2O_3 and NiV-LDH at NF were used as working electrodes. For OER, the commercial Hg/HgO, and Pt ring were used as a reference and counter electrodes respectively, and for HER commercial Hg/HgO, and graphite were used as a reference and counter electrodes respectively in 1 M KOH solution. For total water splitting, NiV-LDH@Mn_2O_3 were used as both cathode and anode.

$$E_{RHE} = E_{ref} + 0.098 + 0.059pH \quad \text{……equation 1}$$

All the potential data were converted into an RHE scale according to the following equation:
all the polarization results have normalized with respect to geometrical surface area The mass and ECSA normalization of all the LSV data was done by using the following relations:

$$\text{ECSA normalization} = \text{Current density} / \text{ECSA} \quad \text{……equation 2}$$

Overpotential

The overpotential values of all the catalysts were calculated at a benchmarking current density of 50 mA cm^{-2} by employing the following relation:

$$\eta_{50}(OER) = (E_{obs} - 1.23)\ V \text{ versus RHE} \quad \text{……equation 3}$$

$$\eta_{50}(HER) = (0 - E_{obs})\ V \text{ versus RHE} \quad \text{……equation 4}$$

The Tafel Slope

The Tafel slope was calculated by fitting the overpotential versus log (j) using the Tafel equation as given below:

$$\eta = b \times \log (j/j_o) \quad \text{……equation 5}$$

where "*b*" signifies the Tafel slope value, "*j*" implies the current density value, and "j_0" is the exchange current density. Electrochemical impedance spectroscopy (EIS) measurements were done on the frequency ranges from 10^5 to 1 Hz.

Electrochemical Active Surface Area (ECSA)

The electrochemical active surface areas (ECSA) were measured by determining the electrochemical C_{dl} using the following equations:

$$i_c = \nu \times C_{dl} \quad \text{……..……equation 6}$$

$$\text{ECSA} = C_{dl}/C_s \quad \text{……equation 7}$$

where "i_c" indicates the double-layer charging current resulting from scan-rates (ν) dependent CVs at non-faradic potential, and "C_s" denotes a specific capacitance value of 0.040 mF cm^{-2} depending on the typical reported values.

Turnover Frequency (TOF):

The turnover frequency (TOF) of all the catalysts have calculated by using the following relation:

$$\text{TOF} = (J \times A) / (n \times F) \quad \text{……equation 8}$$

where "J" stands for the measured current density value at a particular overpotential value, "A" is the geometrical surface area of the working electrode (1 cm^2), and "n" stands for the number of electron transfers (For OER, n = 4 and HER, n = 2), "F" is the Faraday constant with a numerical value of 96 485 C mol^{-1}.

Determination of Surface concentration of all the catalyst from the redox features of CV

- Calculated area associated with the reduction of Ni^{3+} to Ni^{2+} of **NiV-LDH** = 0.002634 VA

Hence, the associated charge is = 0.002634 VA / 0.005 Vs^{-1}

= 0.5268 As

= **0.5268 C**

Now, the number of electron transferred is = 0.5268 C / 1.602 $\times 10^{-19}$

= $\mathbf{0.3288 \times 10^{19}}$

Since, the reduction of Ni^{3+} to Ni^{2+} is a single electron transfer reaction, the number electron calculated above is exactly the same as the number of surface-active sites.

- Calculated area associated with the reduction of Ni^{3+} to Ni^{2+} of $\mathbf{Mn_2O_3}$ = 0.0007806 VA

Hence, the associated charge is = 0.0007806 VA / 0.005 Vs^{-1}

= 0.15612 As

= **0.15612 C**

Now, the number of electron transferred is = 0.15612 C / 1.602 $\times 10^{-19}$

= $\mathbf{0.09745 \times 10^{19}}$

- Calculated area associated with the reduction of Ni^{3+} to Ni^{2+} of **NiV-LDH@**$\mathbf{Mn_2O_3}$ = 0.014505 VA

Hence, the associated charge is = 0.014505 VA / 0.005 Vs^{-1}

= 2.901 As

= **2.901 C**

Now, the number of electron transferred is = 2.901 C / 1.602 $\times 10^{-19}$

= $\mathbf{1.81 \times 10^{19}}$

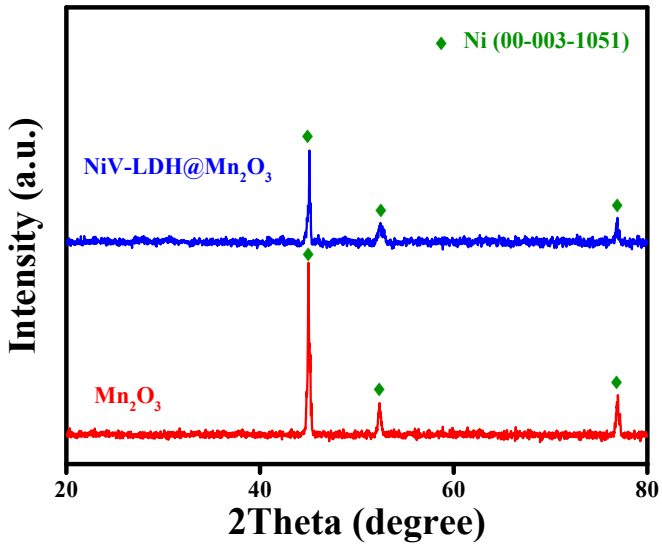

Figure S1: PXRD pattern of Mn_2O_3 and NiV-LDH@Mn_2O_3 at NF substrate.

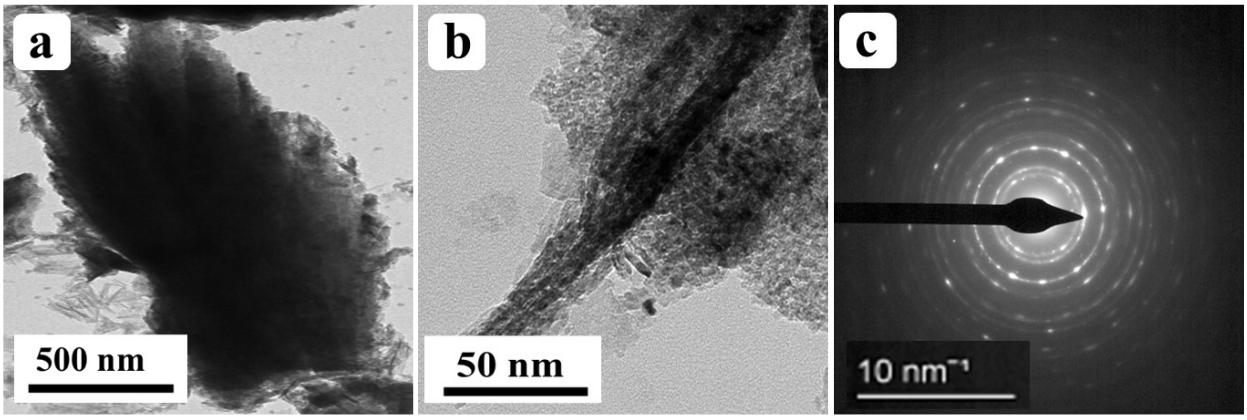

Figure S2: (a and b) low to high magnified HR-TEM NiV-LDH@Mn_2O_3; (c) corresponding SAED pattern

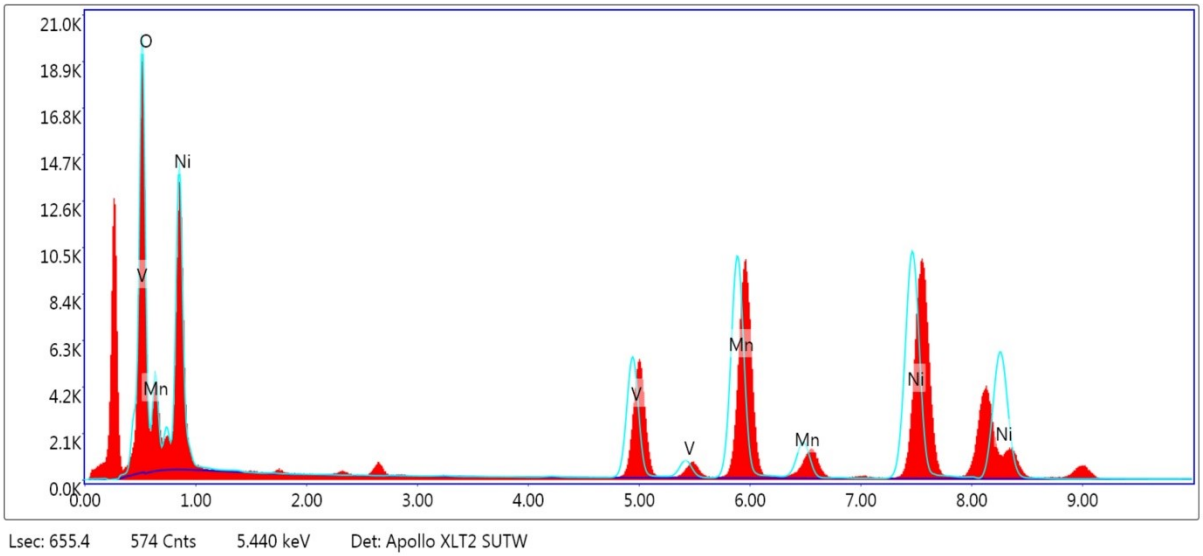

Figure S3: EDS spectrum of NiV-LDH@Mn_2O_3 at HR-TEM mode.

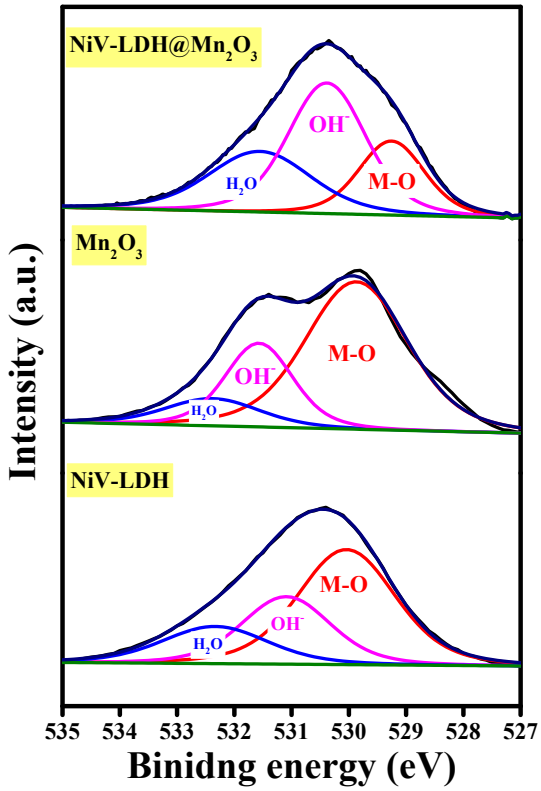

Figure S4: Deconvoluted O 1s XPS spectrum of stacked NiV-LDH, Mn_2O_3 and NiV-LDH@Mn_2O_3.

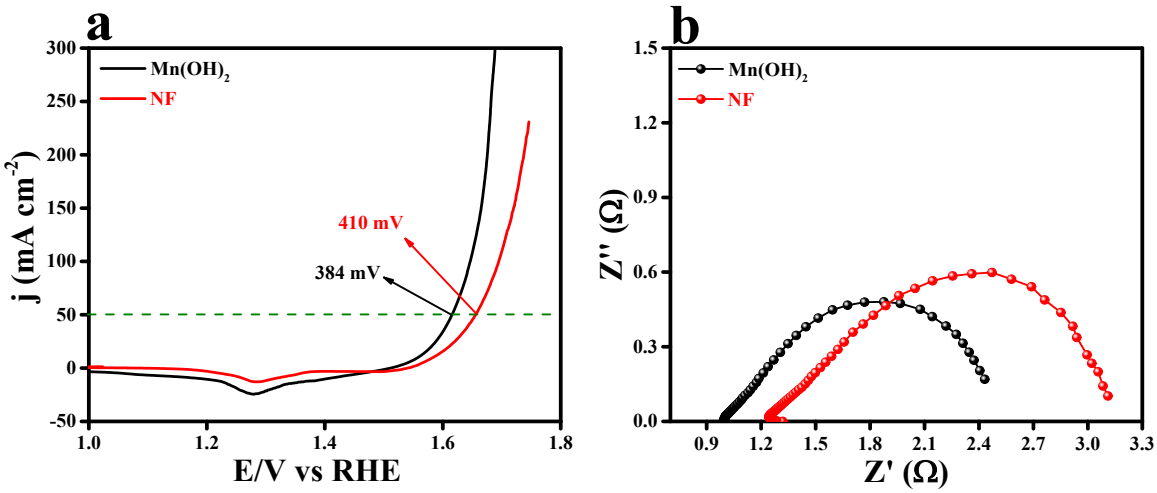

Figure S5: LSV polarization results of $Mn(OH)_2$, NF; (b) corresponding EIS analysis.

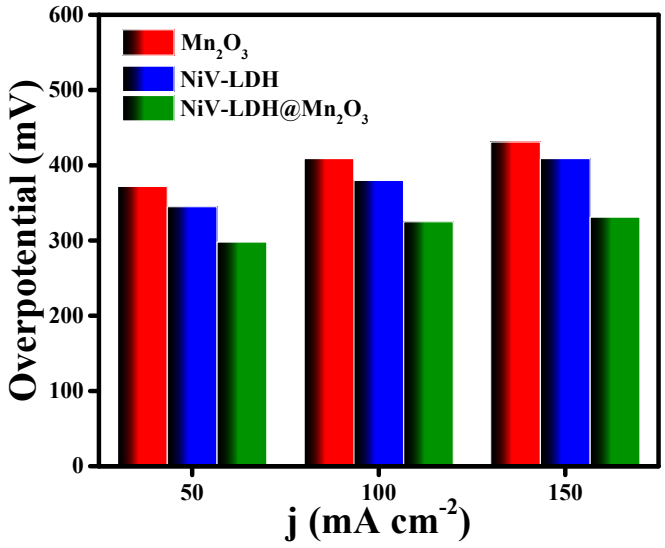

Figure S6: Comparison of overpotentials at different current densities 50, 100 and 150 mA cm^{-2}.

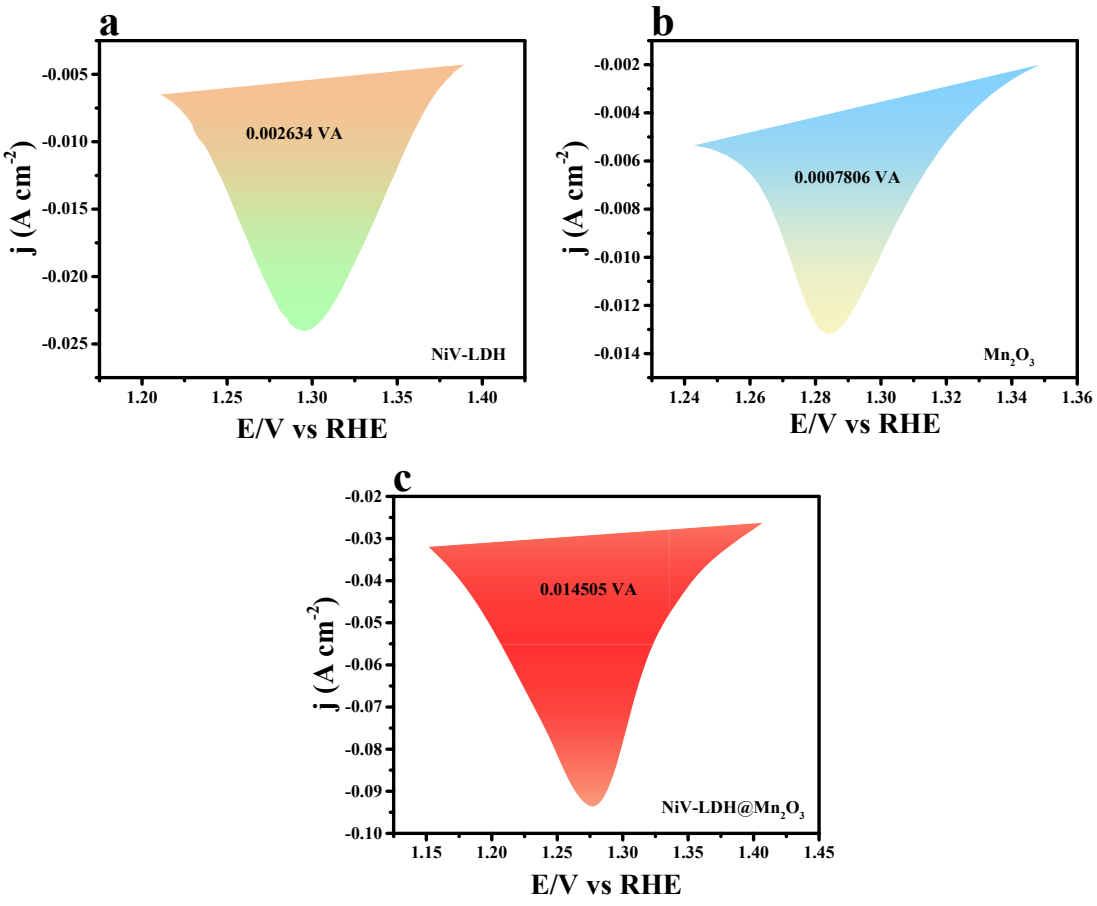

Figure S7: (a-c) Determination of area for reduction peaks of NiV-LDH, Mn_2O_3 and NiV-LDH@Mn_2O_3 respectively.

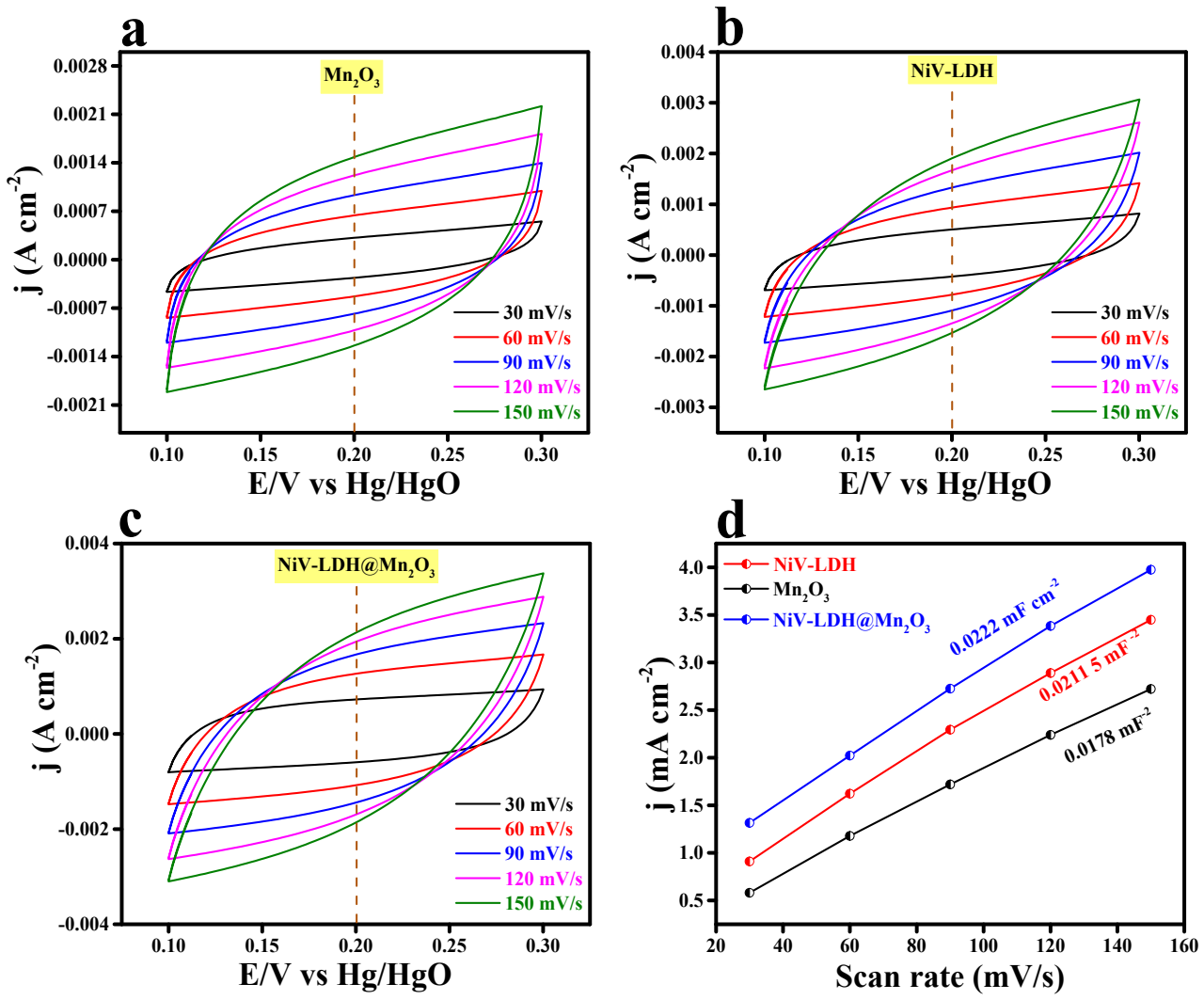

Figure S8: (a-c) shows the CVs recorded for Mn_2O_3, NiV-LDH, and NiV-LDH@Mn_2O_3 in a non-faradaic region at various scan rate for the determination of ECSA from its double layer capacitance in 1 M KOH solution, respectively; (d) corresponding calculated C_{dl} values.

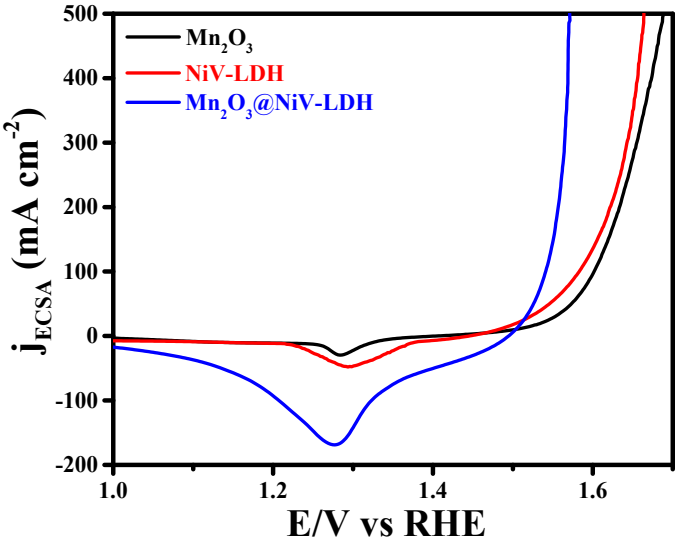

Figure S9: (a-c) ECSA normalized LSV polarization result of Mn_2O_3, NiV-LDH, and NiV-LDH@Mn_2O_3.

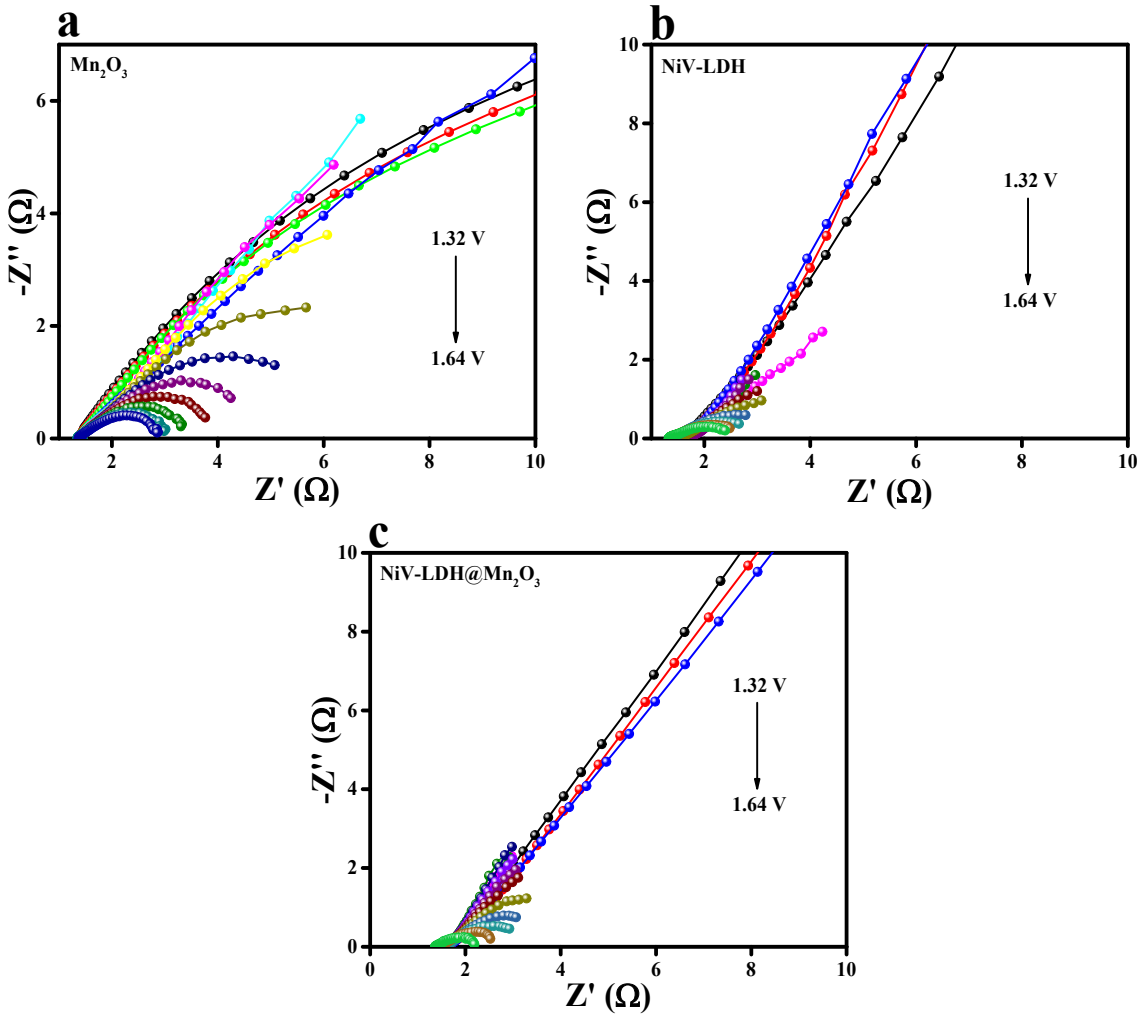

Figure S10: (a-c) Nyquist plots of Mn_2O_3, NiV-LDH, and NiV-LDH@Mn_2O_3 respectively.

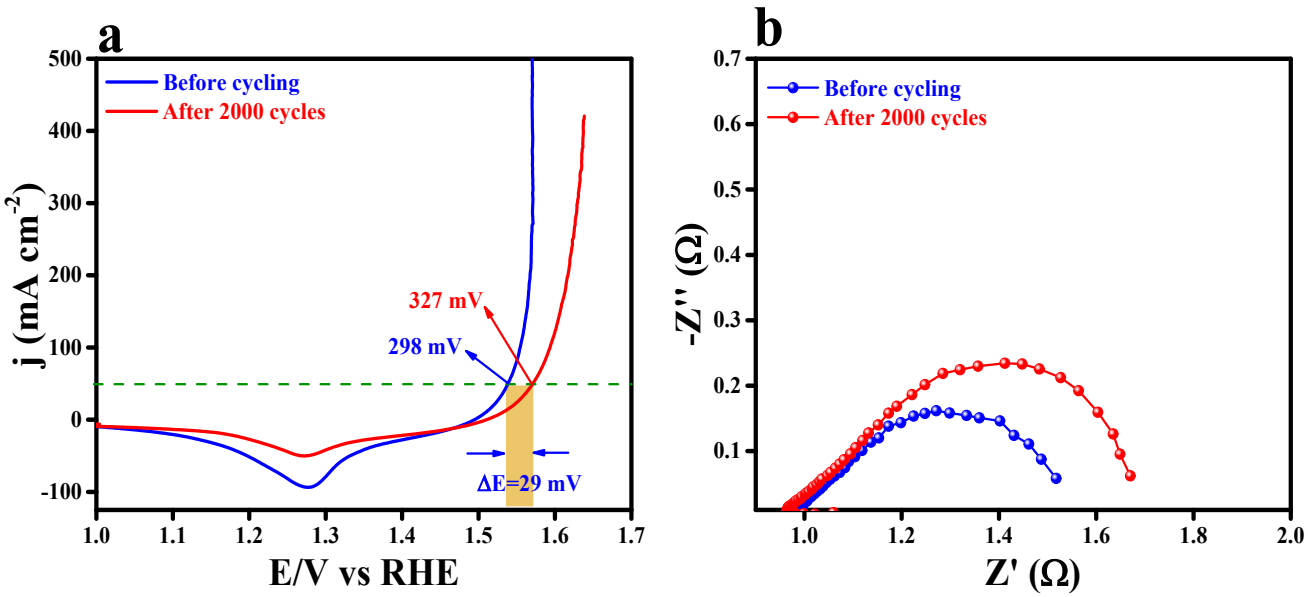

Figure S11: (a) LSV polarization studies of NiV-LDH@Mn_2O_3 heterostructure after 2000 CV cycles towards OER; (b) corresponding EIS analyses at 0.75 V vs Hg/HgO.

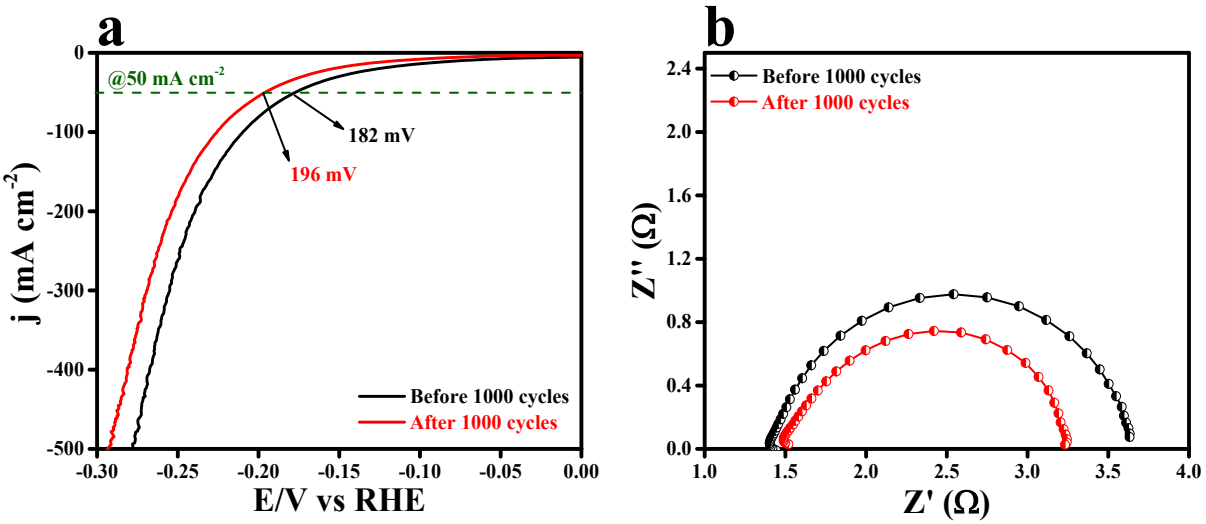

Figure S12: (a) LSV polarization studies of NiV-LDH@Mn_2O_3 heterostructure after 1000 CV cycles towards HER; (b) corresponding EIS analyses at -1.25 V vs Hg/HgO.

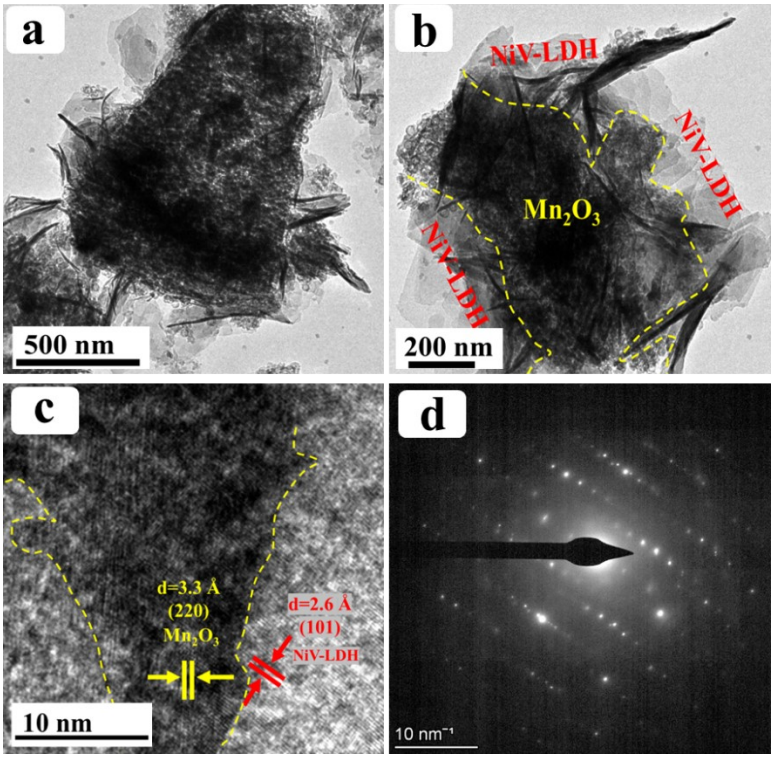

Figure S13: (a-c) Low to high magnified HR-TEM image of NiV-LDH@Mn_2O_3 heterostructure after OER analysis; (s) corresponding SAED pattern.

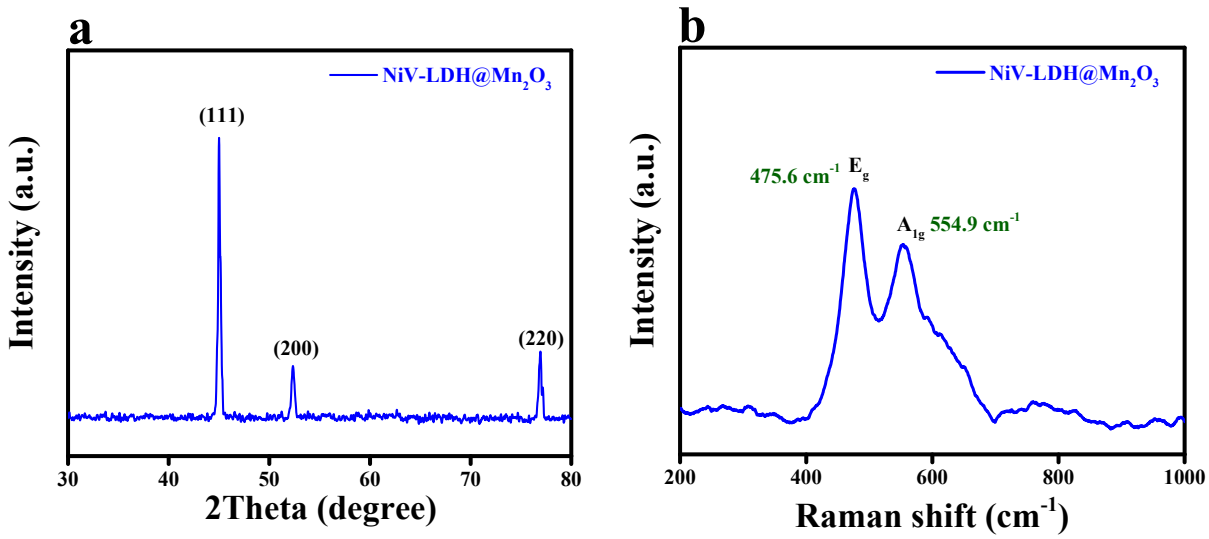

Figure S14: (a and b) Post XRD pattern and Raman spectrum of NiV-LDH@Mn_2O_3 heterostructure after OER studies in 1 M KOH solution.

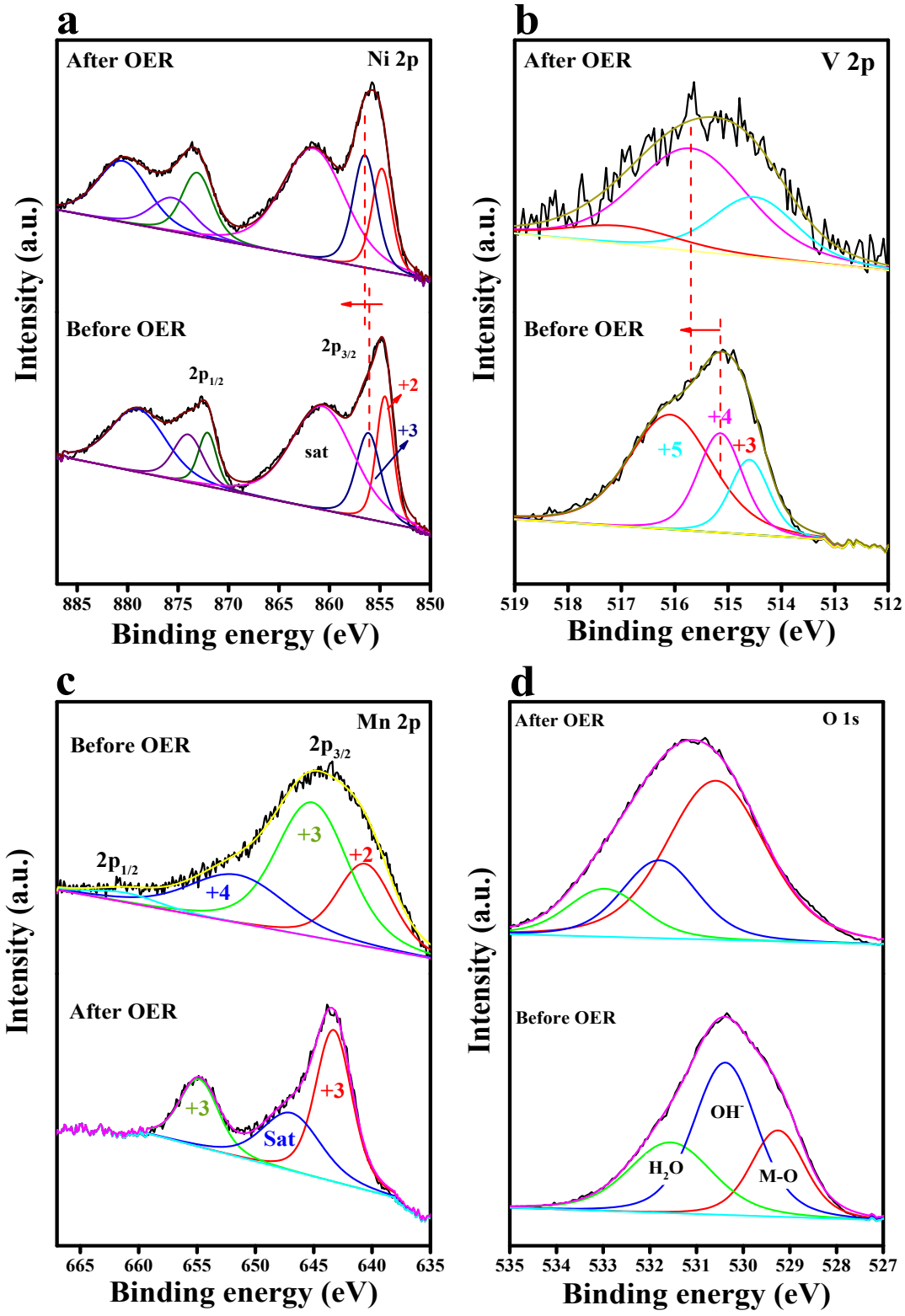

Figure S15: Deconvoluted XPS spectrum of Ni, V, Mn and O of NiV-LDH@Mn_2O_3 heterostructure before and after OER studies in 1 M KOH solution.

S.No	Electrocatalyst	Substrate	Overpotential (mV)	Current density (mA cm^{-2})	Reference
1	NiV-LDH@FeOOH	NF	297	100	1
2	Ru@NiV-LDH	CC	272	10	2
3	Fe_2O_3–Mn_2O_3	NF	350	10	3
4	Ni_3S_2@NiV-LDH	NF	190	10	4
5	CoS@NiV-LDH	NF	274	10	5
6	AD-Mn_2O_3	Graphite sheet	560	10	6
7	Mn_2O_3	NF	270	10	7
8	Mn_2O_3 /RuO_2/Ru	Titanium wire	310	10	8
9	Mn_2P-Mn_2O_3	NF	330	100	9
10	**NiV-LDH@Mn_2O_3**	**NF**	**298**	**50**	**This work**

Table S1: Comparison of NiV-LDH@Mn_2O_3 based electrocatalyst with our catalyst for OER application in 1 M KOH electrolyte solution.

S.No	Electrocatalyst	Substrate	Overpotential (mV)	Current density (mA cm^{-2})	Reference
1	Ru@NiV-LDH	CC (0.5 M H_2SO_4)	135	10	2
2	NiVFe LDHs@NF	NF	117	10	10
3	NiVRu-R	NF	48	100	11
4	Ni_3S_2@NiV-LDH/NF	NF	126	10	4
5	CoS@NiV-LDH	NF	174	50	5
6	Mn_2P-Mn_2O_3	NF	98	10	9
7	**NiV-LDH@Mn_2O_3**	**NF**	**182**	**50**	**This work**

Table S2: Comparison of NiV-LDH@Mn_2O_3 based electrocatalyst with our catalyst for HER application in 1 M KOH electrolyte solution.

S.No	Electrocatalyst	Substrate	Cell voltage (V)	Current density (mA cm^{-2})	Reference
1	NiVIr-LDH||NiVRu-LDH	NF	1.42	10	12
2	Ni_3S_2@NiV-LDH/NF	NF	1.53	10	4
3	Mn_2P-Mn_2O_3	NF	1.65	10	9
4	CoS@NiV-LDH	NF	1.57	10	5
5	NiV-LDH@Mn_2O_3	NF	1.604	10	This work

Table S3: Comparison of cell voltage of NiV-LDH@Mn_2O_3 heterostructure with the similar type of heterostructure electrocatalyst in 1 M KOH electrolyte solution.

References

1 W. Bao, L. Xiao, J. Zhang, Z. Deng, C. Yang, T. Ai and X. Wei, *Chem. Commun.*, 2020, **56**, 9360–9363.

2 A. Karmakar, K. Karthick, S. S. Sankar, S. Kumaravel, R. Madhu, K. Bera, H. N. Dhandapani, S. Nagappan, P. Murugan and S. Kundu, *J. Mater. Chem. A*, 2022, **10**, 3618–3632.

3 C. Maccato, L. Bigiani, T. Andreu, A. Gasparotto, C. Sada, E. Modin, O. I. Lebedev, J. R. Morante and D. Barreca, *ACS Appl. Nano Mater.*, 2020, **3**, 9889–9898.

4 Q. Liu, J. Huang, Y. Zhao, L. Cao, K. Li, N. Zhang, D. Yang, L. Feng and L. Feng, *Nanoscale*, 2019, **11**, 8855–8863.

5 R. Madhu, R. Jayan, A. Karmakar, S. S. Selvasundarasekar, S. Kumaravel, K. Bera, S. Nagappan, H. N Dhandapani, M. M. Islam and S. Kundu, *ACS Sustain. Chem. Eng.*, 2022, **10**, 11299–11309.

6 R. K. Kunchala, Pushpendra, R. Kalia and B. S. Naidu, *ACS Appl. Nano Mater.*, 2021, **4**, 396–405.

7 P. P. Liu, Y. Q. Zheng, H. L. Zhu and T. T. Li, *ACS Appl. Nano Mater.*, 2019, **2**, 744–749.

8 M. P. Browne, H. Nolan, B. Twamley, G. S. Duesberg, P. E. Colavita and M. E. G. Lyons, *ChemElectroChem*, 2016, **3**, 1847–1855.

9 X. Wang, G. Huang, Z. Pan, S. Kang, S. Ma, P. K. Shen and J. Zhu, *Chem. Eng. J.*, 2022, **428**, 131190.

10 X. Ma, S. Zhang, Y. He, T. He, H. Li, Y. Zhang and J. Chen, *J. Electroanal. Chem.*, , 2021, **886**, 115107.

11 X. Chen, J. Wan, M. Zheng, J. Wang, Q. Zhang, L. Gu, L. Zheng, X. Fu and R. Yu, *Nano Res.*, 2023, **16**, 4612–4619.

12 D. Wang, Q. Li, C. Han, Q. Lu, Z. Xing and X. Yang, *Nat. Commun.*, 2019, **10**, 1–12.